Chemistry–A European Journal
Research Article
doi.org/10.1002/chem.202500849
Chemistry Europe
European Chemical Societies Publishing
www.chemeurj.org

Designed Metal-Free Quasi-1D Crystals with Giant Birefringence

Yang Li,[a] Jihyun Lee,[a] and Kang Min Ok*[a]

Birefringence, a vital property of anisotropic crystals, is indispensable for advanced optical technologies. Quasi-1D structures, with their inherent structural anisotropy, offer fertile ground for discovering materials with exceptional optical anisotropy. In this work, we report four metal-free quasi-1D crystals—$(C_5H_6NO)^+(NO_3)^-$(**4HPN**), $(C_5H_6NO)^+(HC_2O_4)^-$(**4HPO**), $(C_4N_3H_6)^+(NO_3)^-$(**2APMN**), and $(C_4N_3H_6)^+(HC_2O_4)^-\cdot H_2O$ (**2APMO**)—designed to feature pseudo-chain structures and grown as centimeter-scale crystals via a facile aqueous-solution method. These crystals display wide bandgaps (3.40–4.48 eV) and exceptional birefringence, with calculated values up to 0.555@546 nm and an experimental maximum of 0.597@546 nm for **4HPN**. The giant birefringence stems from their quasi-1D architectures, high-spatial density, and optimal arrangement of the birefringence-active groups (BAGs). This study highlights the promise of metal-free quasi-1D materials for next-generation miniaturized polarization optics and laser-driven applications.

1. Introduction

Low-dimensional structures with inherent structural anisotropy have attracted significant attention for their potential applications in electronics, optoelectronics, and ion storage systems.[1–4] Among these, birefringence—an optical property arising from anisotropy—is a key feature in the quest for new optical materials.[5–10] Larger birefringence enables more effective splitting of ordinary and extraordinary rays, paving the way for miniaturization of optical devices and expanding their use in laser technologies.[11–13] However, the birefringence values of most reported (quasi–) 2D materials are relatively small, prompting researchers to focus on (quasi–) 1D systems.[14–16]

Recent studies have uncovered quasi-1D materials with exceptionally high birefringence values, such as fibrous red phosphorus (0.642@475 nm), $BaTiS_3$ (0.76), $I^+(C_6H_4NO_2)^-$ (0.778@550 nm), and ZrS_3 (0.76@500 nm).[17–20] Despite this progress, the development of UV birefringent materials remains challenging. Ideal candidates should possess properties such as a large bandgap ($\geq$ 3.10 eV), high birefringence ($\sim$0.4 or higher), ease of crystal growth, and environmental friendliness.[21–23] However, commercial UV birefringent materials are often limited by low birefringence values ($<$0.3), difficulties in growing large crystals, and their inability to meet the demands of applications.[24–26]

To date, several newly reported UV birefringent materials exhibit birefringence values greater than 0.4.[27–33] However, in metal-containing compounds, pollution arising from metal extraction, processing, and disposal—along with higher costs and challenges in crystal growth—highlights the urgent need for environmentally friendly birefringent materials with favorable growth habits, high birefringence, and low cost.[34–37]

Beyond dimensionality, birefringence is influenced by factors such as anisotropic polarizability ($\Delta\alpha$), spatial density (ρ), and the distribution of birefringence-active groups (BAGs).[38–42] Groups with anisotropic electron clouds, such as π-conjugated groups, second-order Jahn-Teller active cations (e.g., Nb^{5+}, Mo^{6+}, Pb^{2+}, Sb^{3+}), and highly deformable d^{10} transition metal cations (e.g., Zn^{2+}, Cd^{2+}, Hg^{2+}), tend to exhibit higher $\Delta\alpha$ values.[43–50] However, to prioritize environmental safety and cost-effectiveness, metal-free quasi-1D systems are of particular interest.

The organic π-conjugated molecule 4-hydroxypyridine (**4HP**) is an excellent BAG owing to its large $\Delta\alpha$, making it a promising building block for birefringent materials, as demonstrated experimentally.[32,38,39,51] It can form corner-sharing structures with various atoms (e.g., Li, Zn, Sb) through oxygen atom or link with other hydrogen acceptors through hydrogen bonds. In pseudo–3D $[Mg(NO_3)_2\cdot 6H_2O](\mathbf{4HP})_2$ (**Mg—4HP**), hydrogen bonding results in the formation of $[\mathbf{4HP}\cdot NO_3^-]$ dimers with small dihedral angles.[38] However, the birefringence-inert $[Mg(H_2O)_6]^{2+}$ obscures this dimer, generating infinite quasi-1D chains.

To address this limitation, we tailored the structure by removing the birefringence-inert $[Mg(H_2O)_6]^{2+}$ group, thereby constructing a metal-free quasi-1D chain of $[(\mathbf{4HP})^+\cdot(NO_3)^-]$. This approach maintains the small dihedral angles and enhances the spatial density of BAGs, achieving high birefringence, low cost, and ease of large-crystal growth. Inspired by this, we also explored 2–aminopyrimidine (**2APM**) and $HC_2O_4^-$, which exhibit

[a] Y. Li, J. Lee, K. M. Ok
Department of Chemistry, Sogang University, Seoul 04107, Republic of Korea
E-mail: kmok@sogang.ac.kr

Supporting information for this article is available on the WWW under https://doi.org/10.1002/chem.202500849

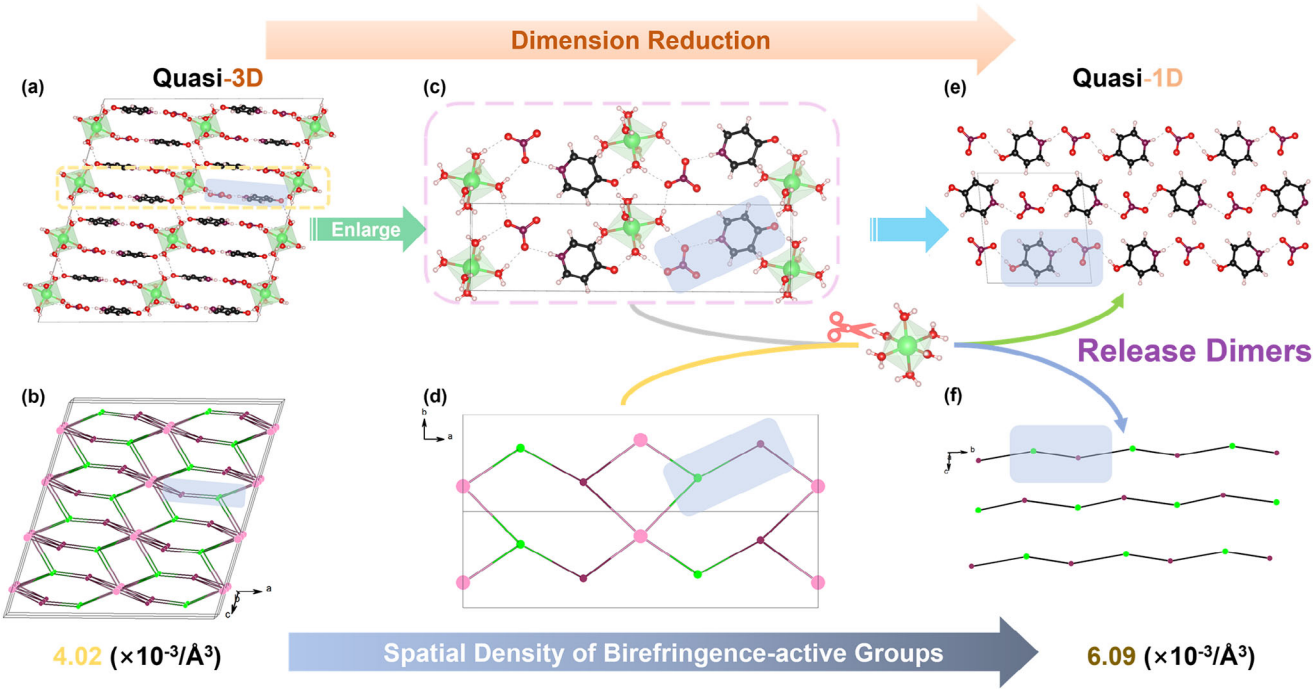

Figure 1. Ball-and-stick models of **Mg—4HP** (a), a selected region of **Mg—4HP** (c), and **4HPN** (C, black; N, purple; O, red; H, white; Mg, green). (b), (d), and (e) show the corresponding topological diagrams ($[Mg(H_2O)_6]^{2+}$, pink; **4HP**/**4HP**$^+$, green; NO_3^-, purple). The highlighted blue region represents the [**4HP**·NO_3^-] and [**4HP**$^+$·NO_3^-] dimers.

larger $\Delta\alpha$ values than **4HP** and NO_3^-, as candidates for new metal-free quasi-1D birefringent materials.

Herein, we successfully designed and synthesized four quasi-1D compounds: (**4HP**)$^+$(NO_3)$^-$ (**4HPN**), (**4HP**)$^+$(HC_2O_4)$^-$ (**4HPO**), (**2APM**)$^+$(NO_3)$^-$ (**2APMN**), and (**2APM**)$^+$(HC_2O_4)$^-$·H_2O (**2APMO**). These compounds were grown as centimeter-scale crystals using a mild aqueous-solution method with high yields (>95%, based on **4HP** or **2APM**). All four materials demonstrated giant birefringence, with **4HPN** achieving an experimental birefringence of 0.597@ 546 nm.

2. Results and Discussion

4HPN crystallizes in the polar space group, *P*1. While preparing this manuscript, we noted that the giant birefringence of the **4HPN** crystal was just reported by Chen and colleagues.[52] The asymmetric unit contains two **4HP**$^+$ cations and two NO_3^- anions. Through N—H···O hydrogen bonding, pseudo–chains of [**4HP**$^+$·NO_3^-] are formed along a specific orientation (Figure 1). The bond distances between C—O (d_{C-O}), C—C (d_{C-C}), and C—N (d_{C-N}) atoms within **4HP**$^+$ fall in the ranges of 1.327(4)–1.330(4), 1.358(5)–1.409(4), and 1.343(4)–1.358(4) Å, respectively. In the case of NO_3^-, the N—O bond lengths range from 1.247(4) to 1.330(4) Å. The dihedral angles between NO_3^- and **4HP**$^+$ range from 1.71 to 11.62°, favorably contributing to birefringence.

4HPO crystallizes in the monoclinic crystal system, with space group $P2_1/c$ and unit cell parameters: a = 5.6877(6) Å, b = 20.879(2) Å, c = 6.9765(8) Å, β = 112.450(3)°, and Z = 4. The $HC_2O_4^-$ anion adopts an end-to-end configuration, forming infinite quasi-1D $[HC_2O_4^-]_n$ chains along the *a*-axis. The C—C and C—O bond lengths in $HC_2O_4^-$ are 1.556(3) and 1.209(2)–1.308(2) Å, respectively. Interestingly, the **4HP**$^+$ cations attach to these $[HC_2O_4^-]_n$ chains via O1—H1···O2 hydrogen bonds, generating neutral [**4HP**$^+$·$HC_2O_4^-$]$_n$ chains (Figures S2 b,c). Within **4HP**$^+$, the C—O, C—N, and C—C bond lengths are 1.325(2), 1.345(2)–1.346(2), and 1.359(2)–1.403(2) Å, respectively. The dihedral angle between $HC_2O_4^-$ and **4HP**$^+$ is 23.56°, partially offsetting their contribution to birefringence.

2APMN crystallizes in the monoclinic crystal system (*C*2/*c* space group).[53] The **2APM**$^+$ cations form both bidentate and monodentate hydrogen bonds with adjacent NO_3^- anions via H···N—O hydrogen bonding interactions, resulting in infinity neutral [**2APM**$^+$·NO_3^-]$_n$ pseudo-chains along the *b*-axis (Figures S2d,e). Similar to **4HPN**, the NO_3^- anion in this structure also adopts a configuration with one shorter and two longer N—O bond lengths, ranging from 1.217(5) to 1.254(5) Å. In the **2APM**$^+$ cation, the C—N and C—C bond lengths are 1.307(6)–1.360(5) and 1.346(7)–1.412(7) Å, respectively. The dihedral angles among NO_3^-—NO_3^-, **2APM**$^+$–**2APM**$^+$, and **2APM**$^+$–NO_3^- are 0.45–12.11°, 0.18–0.58°, and 5.60–6.41°, respectively.

2APMO crystallizes in the triclinic crystal system (*P*-1 space group).[54] The **2APM**$^+$ cations form bidentate and monodentate hydrogen bonds with adjacent $HC_2O_4^-$ anions via H···O—C hydrogen bonding interactions, leading to infinity neutral [**2APM**$^+$·$HC_2O_4^-$]$_n$ pseudo-single-chains along the *a*-axis.

Besides, H_2O molecules serve as both hydrogen-bond donors and acceptors, assembling the pseudo-single chains into step-shaped pseudo-single chains of [(**2APM**$^+$·$HC_2O_4^-$·H_2O)$_2$]$_n$ (Figures S2f–g). The dihedral angles among $HC_2O_4^-$–$HC_2O_4^-$,

2APM^{+}–**2APM**$^{+}$, and **2APM**$^{+}$–$HC_2O_4^-$ are 0–0.05°, 0°, and 2.49–2.50°, respectively. Hydrogen bonding and π–π interactions were visualized using the IGMH method, as shown in Figure S6.

The Infrared (IR) spectra further confirmed their structures (Figure S7).[55,56] The ultraviolet-visible (UV-vis) diffuse reflectance spectra (Figure S8a) and UV-near infrared (NIR) transmittance spectra (Figure S8b) reveal their UV cutoff edges of 252, 300, 341, and 340 nm for **4HPN**, **4HPO**, **2APMN**, and **2APMO**, respectively. The corresponding experimental bandgaps are 4.48, 4.13, 3.65, and 3.40 eV, as shown in Figure S9. The underestimated bandgaps are attributed to the discontinuity of the exchange-correlation energy.[57,58] The difference between the experimental and calculated bandgaps is applied as a "scissor" operator to analyze the birefringence. The absorption band around 300 nm in **4HPN** is induced by NO_3^-, consistent with previous reports.[59–61]

Powder second-harmonic generation (SHG) measurements for polycrystalline **4HPN** indicate type-I phase-matching behavior, with a significant SHG response of 2 × KDP, comparable to recently reported work (Figure S10).[52]

Thermogravimetric analysis (TGA) curves show that **4HPN**, **4HPO**, **2APMN**, and **2APMO** remain stable up to 200, 200, 150, and 75 °C, respectively (Figure S11). Notably, **4HPN**, **4HPO**, and **2APMN** exhibit excellent stability, retaining their integrity even after over 2 years of exposure to air. In contrast, **2APMO** shows efflorescence due to the loss of lattice H_2O molecules. Moreover, a straightforward approach to enhancing thermal stability is to select covalent bonds that connect these BAGs effectively.[62–64]

The calculated bandgaps (using GGA/PBE–TS) for **4HPN**, **4HPO**, **2APMN**, and **2APMO** are 3.73, 3.35, 2.78, and 2.97 eV, respectively (Figure S12). To achieve more accurate bandgap predictions, the HSE06 hybrid functional was applied, yielding bandgaps of 4.54 and 4.24 eV for **4HPN** and **4HPO**, which align well with the experimental values of 4.48 and 4.13 eV, respectively.

As shown in Figure S13, the density of states (DOS) analysis indicates that both the organic cations and anions contribute significantly to the optical properties of these compounds. The calculated birefringence values for these quasi-1D metal-free compounds are remarkable, with 0.555, 0.500, 0.541, and 0.533 at 546 nm for **4HPN**, **4HPO**, **2APMN**, and **2APMO**, respectively (Figure S14).

The highest occupied crystal orbital (HOCO) and lowest unoccupied crystal orbital (LUCO) of **4HPN** (Figures 2a-b) reveal that the HOCO is primarily dominated by NO_3^-, while the LUCO is mainly governed by **4HP**$^{+}$. The localized orbital locator-π (LOL-π) diagrams (Figures 2c and S15) illustrate that the out-of-plane delocalized π electrons are perpendicular to the in-plane coplanar groups. This configuration creates a significant anisotropic difference in electron density between the out-of-plane and in-plane regions, ultimately leading to pronounced optical anisotropy (birefringence). The electron localization function (ELF) diagrams confirm that both the 6-membered ring (6-MR) cations (**4HP**$^{+}$ and **2APM**$^{+}$) and the anions ($HC_2O_4^-$ and NO_3^-) exhibit strong π-conjugated structural features, which are the primary contributors to the observed birefringence (Figures 2d and S16). Interestingly, in the **2APMO**, H_2O molecules also make a measurable contribution to birefringence.

The proper **4HPN** and two additional crystals, **4HPO** and **2APMO**, with their (001) planes, were selected to measure birefringence using the polarized microscope method (Figures 3, S17 and S19). The optical path differences were measured as 4.170, 7.117, and 8.463 μm for **4HPN**, **4HPO**, and **2APMO**, respectively. The corresponding birefringence values at 546 nm are 4.170/6.98 = 0.597 for **4HPN**, 7.117/23.75 = 0.300 for **4HPO** (in the (001) plane), and 8.463/21.274 = 0.398 for **2APMO** (in the (001) plane). These experimental birefringence values are in close agreement with the calculated values of 0.555@546 nm for **4HPN**, 0.315@546 nm for **4HPO** in the (001) plane, and 0.418@546 nm for **2APMO** in the (001) plane (Figures S14, S18, and S20).

The giant birefringence of the metal-free **4HPN** far exceeds that of commercial birefringent materials such as α-BaB_2O_4, $CaCO_3$, and YVO_4, and is comparable to the metal-free birefringent material $NH_4(H_2C_6N_7O_3)\cdot 2H_2O$ (Exp. 0.54@550 nm).[24–26,34] Moreover, this value surpasses those of other reported **4HP**-based compounds, such as the template **Mg—4HP**, $[LiNO_3\cdot H_2O\cdot$**4HP**$]\cdot$**4HP** (**Li—4HP2**), (**4HP**)$_2ZnCl_2$ (**ZnCl$_2$—4HP**), $(C_5H_5NO)(Sb_2OF_4)$, and most UV 6-MRs-based compounds, including $(C_3N_6H_7)_2[B_3O_3F_4(OH)]$ and $Cs_3Cl(HC_3N_3S_3)$.[29,30,32,38,39] As revealed in Figure 4, these four compounds keep good balance of giant birefringence, wide bandgaps, and ease of large-crystal growth, thus promising UV birefringent crystals for further application.[65–70]

The remarkable birefringence (≥0.5@546 nm) observed in these four compounds prompted a deeper investigation into origins through theoretical calculations and structural analysis. Structurally, three key factors contribute to the large birefringence:

1. Quasi-chain structures: These exhibit significant anisotropy between the in-chain/plane and out-of-chain/plane, which enhances birefringence.
2. Smaller dihedral angles: Reduced dihedral angles between coplanar cations and anions significantly contribute to birefringence.
3. Higher spatial density of BAGs: Increased spatial density is essential for achieving giant birefringence.

To explore these factors in detail, the template compound **Mg—4HP** and **4HPN** were selected for comparison. In both structures, NO_3^- and **4HP**/**4HP**$^{+}$ serve as BAGs with comparable dihedral angles (1.45–14.88° for **Mg—4HP** and 1.71–11.62° for **4HPN**). However, the spatial density of BAGs plays a dominant role in the significant birefringence difference. By replacing the birefringence-inert $[Mg(H_2O)_6]^{2+}$ groups, the spatial density of NO_3^- and **4HP** in **4HPN** increases by approximately 51.5% (from 4.02 × 10^{-3}/Å^3 in **Mg—4HP** to 6.09 × 10^{-3}/Å^3 in **4HPN**). This enhancement correlates well with the observed birefringence increase from 0.376 to 0.597@546 nm, representing a 58.8% improvement.

These results indicate that large birefringence primarily originates from the high-spatial density of BAGs. However, the contribution of individual components is not yet fully understood. To address this, we applied a previously established model

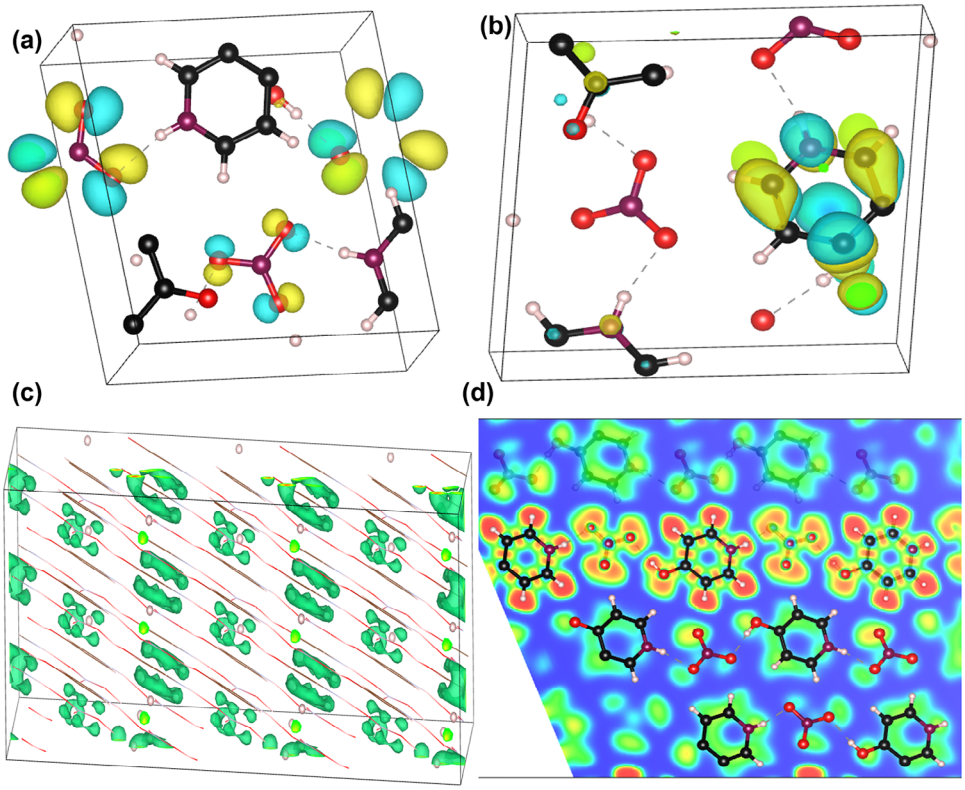

Figure 2. HOCO (a) and LUCO (b) orbitals, LOL-π (c), and ELF (d) diagrams for selected regions of **4HPN**.

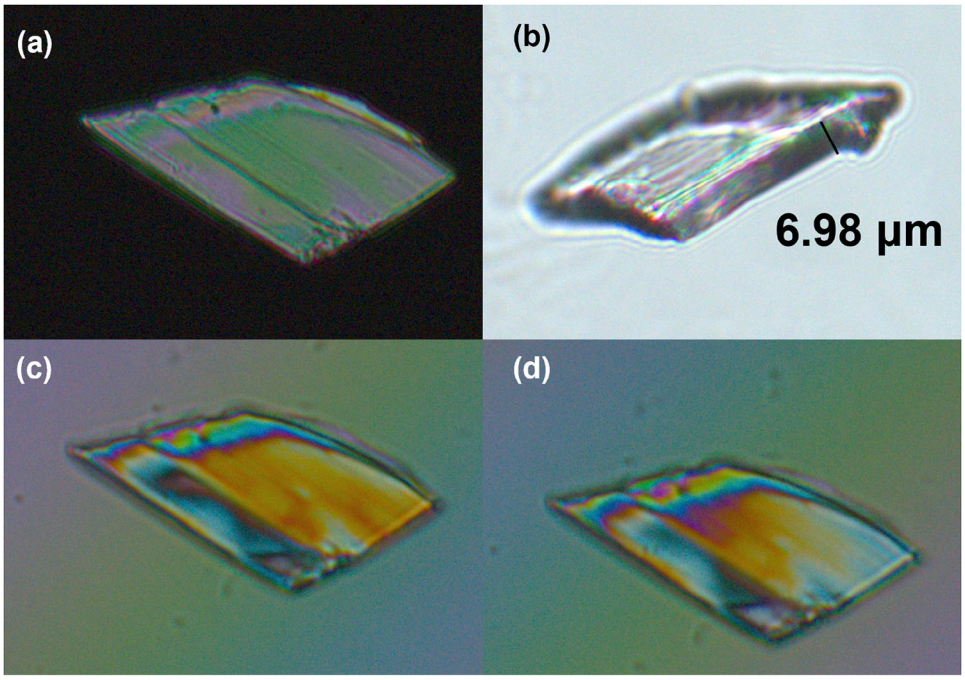

Figure 3. Selected **4HPN** crystal observed under cross-polarized light, showing complete extinction under a polarizing microscope (a, c, d), along with its thickness measurement (b).

to semi-quantitatively evaluate their contributions. Based on this model, the deduced birefringence values at 546 nm are 0.562, 0.526, 0.560, and 0.486 for **4HPN**, **4HPO**, **2APMN**, and **2APMO**, respectively. These values align closely with the calculated birefringence values of 0.555, 0.500, 0.541, and 0.533 (Figure 5).

The slightly larger deviation observed for **2APMO** suggests that the contribution from H_2O cannot be ignored, as revealed

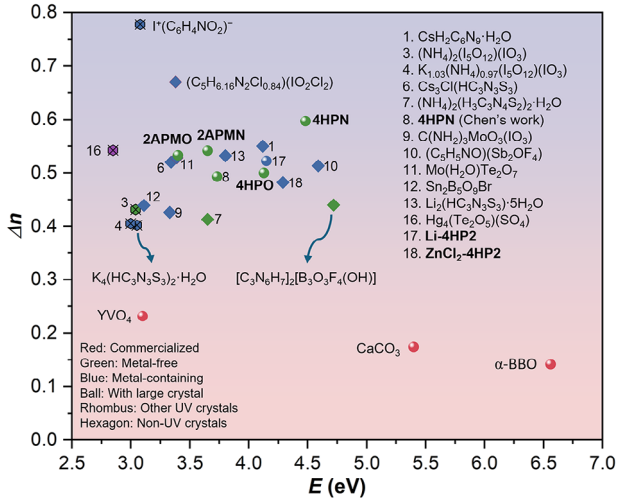

Figure 4. Selected birefringent materials (≥0.4) compared with commercial birefringent materials.

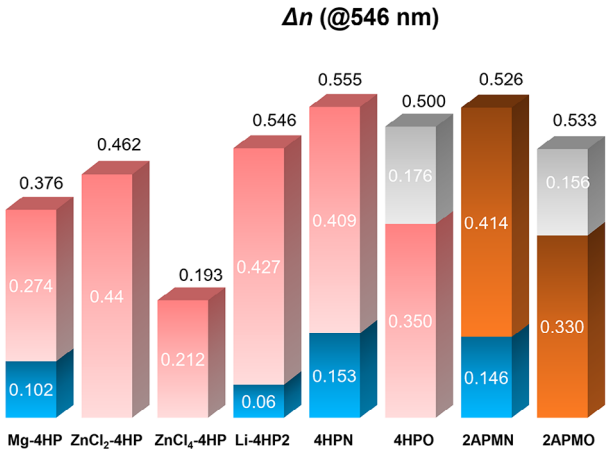

Figure 5. Deduced and calculated birefringence (@546 nm) of previously reported **4HP**-based birefringent crystals and the compounds studied in this work. Blue: NO_3^-, Red: **4HP**/**4HP**$^+$; Gray: $HC_2O_4^-$; Brown: **2APM**$^+$. White values represent the deduced contributions to birefringence, while black values indicate the calculated birefringence. **Li—4HP2** refers to [$LiNO_3$·H_2O·**4HP**]·**4HP**, **$ZnCl_2$—4HP** to (**4HP**)$_2ZnCl_2$, and **$ZnCl_4$—4HP** to (**4HP**$^+$)$_2$($ZnCl_4^{2-}$).

by the ELF diagrams. In addition, among compounds with the same spatial density of BAGs, organic cations with larger $\Delta\alpha$ contribute more significantly to birefringence.

3. Conclusions

In summary, four tailor-made quasi-1D metal-free compounds, **4HPN**, **4HPO**, **2APMN**, and **2APMO**, were successfully designed and grown as centimeter-sized crystals under mild aqueous-solution conditions. These compounds consist of 6-MR cations (**4HP**$^+$ and **2APM**$^+$) and π-conjugated anions ($HC_2O_4^-$ and NO_3^-) with high-spatial densities of BAGs. Benefiting from their quasi-1D structures, nearly parallel alignment of components, and high-spatial density of BAGs, these compounds exhibit giant birefringence values ranging from 0.500 to 0.597@546 nm. Further analysis confirms that the 6-MR cations (**4HP**$^+$ and **2APM**$^+$) play a dominant role in generating the large birefringence, as expected. With their ease of growth into large crystals, wide bandgaps, and high birefringence, **4HPN**, **4HPO**, **2APMN**, and **2APMO** emerge as promising candidates for UV-birefringent materials. This work also provides valuable insights into the design of novel metal-free quasi-1D compounds with exceptional birefringence.

4. Experimental Section

Single crystal growth: 4-Hydroxypyridine (**4HP**) (TCI, >99%), **2APM** (ACROS, 98%), $H_2C_2O_4$ (Alfa Aesar, 98%), and HNO_3 (SAMCHUN, w.t. 60.0%) were used as received. A total of 0.951 g of **4HP** (**2APM**) was dissolved in 50 mL of distilled water in a plastic beaker. For **4HPN** (**2APMN**), 5 mL of HNO_3 was added, while for **4HPO** (**2APMO**), 0.602 g of $H_2C_2O_4$ was used. These solutions were slowly evaporated at room temperature for 1 week, resulting in centemeter-sized crystals, which were washed with distilled water. Polycrystalline samples were prepared by grinding the as-grown crystals and analyzed using powder X-ray diffraction.

Characterization: Powder X-ray diffraction data were collected using a MiniFlex 600 diffractometer with Cu Kα radiation (λ = 1.54406 Å), operating at 40 kV and 15 mA at room temperature. The sample was scanned in the 2θ range of 5–70° with a scan speed of 5 °/minute and a step size of 0.02°. The measured diffraction patterns of the compounds matched well with the simulated results (Figure S1).

Crystals of suitable size were selected for structure determination using a Bruker D8 QUEST diffractometer with a Mo Kα-radiation source (λ = 0.71073 Å) at the Advanced Bio-Interface Core Research Facility, Sogang University. For **4HPN**, **4HPO**, **2APMN**, and **2APMO**, single-crystal data were collected at 109 K, 120 K, 260 K, and 244 K, respectively.[71] Data reduction and absorption correction were performed using the SAINT and SADABS programs, respectively.[72] The structure were solved and refined using the OLEX2 package,[73] and the solved structures were checked for missing higher symmetry using PLATON.[74] Crystallographic data, structure refinement details, atomic coordinates, equivalent isotropic displacement parameters, and selected bond lengths and angles are provided in the Supporting Information (Tables S1–S6).

IR spectra were recorded in the range of 500–4000 cm^{-1} using a Thermo Scientific Nicolet iS50 FT-IR spectrometer. The ground samples were placed on a diamond attenuated total reflectance crystal (Figure S7).

The UV-vis diffuse-reflectance spectra of **4HPN**, **2APMN**, and **2APMO** were recorded using a Lambda 1050 scan UV-vis spectrophotometer at room temperature over the wavelength range of 200–800 nm (Figure S8a). The reflection spectra were converted to absorbance date using the Kubelka-Munk function (Figure S9).[75] UV-vis-NIR transmittance spectra for unpolished brittle **4HPO** and **2APMN** crystals were measured using a Shimadzu SolidSpec-3700 DUV spectrophotometer at room temperature, covering the wavelength range of 200–1600 (Figure S8b).

Experimental birefringence measurements were conducted using a ZEISS Axiolab5 polarizing microscope equipped with a Berek compensator at 546 nm (Figures 3, S17, and S19). Crystal orientation was determined with a Bruker D8 QUEST diffractometer. However, due to the small size of the selected **4HPN** crystal used for birefringence measurements, the harvested diffraction spots were insufficient to precisely determine its orientation.

Powder SHG measurements of **4HPN** were performed using a modified Kurtz-Perry NLO system with a DAWA Q-switched Nd:YAG laser emitting 1064 nm radiation.[76] The crystals were finely ground and sieved into various particle-size ranges: 0–20, 20–45, 45–63, 63–75, 75–90, 90–125, 125–150, 150–200, and 200–250 μm. KH_2PO_4 (KDP) was used as the reference standard (Figure S10).

TGA was carried out using a SCINCO TGA-N 1000 thermal analyzer. Ground polycrystalline samples were loaded into alumina crucibles and heated up to 900 °C at a rate of 10 °C min^{-1} under flowing Ar gas (Figure S11).

The CASTEP package (version 24.1) was used for first-principles calculations based on density-functional theory.[77] Band structures, DOS, and optical properties were calculated using the Perdew-Burke-Ernzerhof (PBE) generalized gradient approximation (GGA) with the TS correction (GGA/PBE-TS) and the norm-conserving pseudopotential (NCP).[78] A plane-wave cut-off energy of 830 eV was selected, and a dense *k*-point sampling with a resolution of less than 0.04 $Å^{-1}$ was adopted. Other parameters were set to the ultra-fine level by default. Polarizability anisotropy was calculated using Gaussian 09 at the B3LYP/6-31G (D3-BJ) level and analyzed with Multiwfn (Table S8).[79–81] CP2K (version 2024.1) was used to calculate the ELF, the LOL-π, Independent Gradient Model based on Hirshfeld partition (IGMH) analyses, and the HOCO and LUCO at the B3LYP/6-31G* (D3-BJ) level (Figures S6, S12-S16, S18, and S20).[82]

Acknowledgments

This research was supported by the National Research Foundation of Korea (NRF) funded by the Ministry of Science and ICT (Grant No. RS-2024-00442105).

Conflict of Interests

The authors declare no conflict of interest.

Data Availability Statement

The data that support the findings of this study are available from the corresponding author upon reasonable request.

Keywords: birefringence · birefringent crystals · DFT calculation · metal-free crystals · quasi-chains crystals

[1] J. Ghosh, S. Parveen, P. J. Sellin, P. K. Giri, *Adv. Mater. Technol.* **2023**, *8*, 2300400.
[2] H. Xu, J. Liu, S. Wei, J. Luo, R. Gong, S. Tian, Y. Yang, Y. Lei, X. Chen, J. Wang, G. Zhong, Y. Tang, F. Wang, H. Cheng, B. Ding, *Light. Sci. Appl.* **2023**, *12*, 278.
[3] Z. Li, T. Yan, X. Fang, *Nat. Rev. Mater.* **2023**, *8*, 587.
[4] A. K. Geim, K. S. Novoselov, *Nat. Mater.* **2007**, *6*, 183.
[5] Y. Li, X. Chen, K. M. Ok, *Chem. Sci.* **2024**, *15*, 15145.
[6] Q. Guo, Q. Zhang, T. Zhang, J. Zhou, S. Xiao, S. Wang, Y. Feng, C. Qiu, *Nat. Photon.* **2024**, *18*, 1170.
[7] H. Qiu, F. Li, C. Jin, Z. Yang, J. Li, S. Pan, M. Mutailipu, *Angew. Chem., Int. Ed.* **2024**, *63*, e202316194.
[8] S. Yang, H. Wu, Z. Hu, J. Wang, Y. Wu, H. Yu, *Small* **2024**, *20*, 2306459.
[9] M. Mutailipu, J. Han, Z. Li, F. Li, J. Li, F. Zhang, X. Long, Z. Yang, S. Pan, *Nat. Photon.* **2023**, *17*, 694–701.
[10] J. Wang, M. Zhu, Y. Chu, J. Tian, L. Liu, B. Zhang, P. S. Halasyamani, *Small.* **2024**, *20*, e2308884.
[11] F. Zhang, X. Chen, M. Zhang, W. Jin, S. Han, Z. Yang, S. Pan, *Light: Sci. Appl.* **2022**, *11*, 252.
[12] X. Chen, B. Zhang, F. Zhang, Y. Wang, M. Zhang, Z. Yang, K. R. Poeppelmeier, S. Pan, *J. Am. Chem. Soc.* **2018**, *140*, 16311.
[13] Y. Zhou, Z. Guo, H. Gu, Y. Li, Y. Song, S. Liu, M. Hong, S. Zhao, J. Luo, *Nat. Photon.* **2024**, *18*, 922.
[14] S. Hou, Z. Guo, T. Xiong, X. Wang, J. Yang, Y. Liu, Z. Niu, S. Liu, B. Liu, S. Zhai, H. Gu, Z. Wei, *Nano Res.* **2022**, *15*, 8579.
[15] H. Yang, H. Jussila, A. Autere, H. P. Komsa, G. Ye, X. Chen, T. Hasan, Z. Sun, *ACS Photonics* **2017**, *4*, 3023.
[16] N. Mao, J. Tang, L. Xie, J. Wu, B. Han, J. Lin, S. Deng, W. Ji, H. Xu, K. Liu, L. Tong, J. Zhang, *J. Am. Chem. Soc.* **2016**, *138*, 300.
[17] W. Chen, B. Zhang, K. Tao, Q. Li, J. Sun, Q. Yan, *Angew. Chem. Int. Ed.* **2024**, *63*, e202403531.
[18] S. Niu, G. Joe, H. Zhao, Y. Zhou, T. Orvis, H. Huyan, J. Salman, K. Mahalingam, B. Urwin, J. Wu, Y. Liu, T. E. Tiwald, S. B. Cronin, B. M. Howe, M. Mecklenburg, R. Haiges, D. J. Singh, H. Wang, M. A. Kats, J. Ravichandran, *Nat. Photon.* **2018**, *12*, 392.
[19] J. Chen, M. B. Xu, H. Y. Wu, J. Y. Wu, K. Z. Du, *Angew. Chem., Int. Ed.* **2024**, *63*, e202411503.
[20] S. Hou, Z. Guo, J. Yang, Y. Liu, W. Shen, C. Hu, S. Liu, H. Gu, Z. Wei, *Small* **2021**, *17*, 2100457.
[21] A. Tudi, S. Han, Z. Yang, S. Pan, *Coord. Chem. Rev.* **2022**, *459*, 214380.
[22] Y. Huang, Y. Zhang, D. Chu, Z. Yang, G. Li, S. Pan, *Chem. Mater.* **2023**, *35*, 4556.
[23] Y. Zhao, L. Zhu, Y. Li, X. Kuang, J. Luo, S. Zhao, *Mater. Chem. Front.* **2023**, *7*, 3986.
[24] G. Zhou, J. Xu, X. Chen, H. Zhong, S. Wang, K. Xu, P. Deng, F. Gan, *J. Cryst. Growth.* **1998**, *191*, 517.
[25] G. Ghosh, *Opt. Commun.* **1999**, *163*, 95.
[26] H. Luo, T. Tkaczyk, R. Sampson, E. L. Dereniak, *Semiconductor Photodetectors III* **2006**, *6119*, 136.
[27] J. Wu, C. Hu, Y. Li, J. Mao, F. Kong, *Chem. Sci.* **2024**, *15*, 8071.
[28] W. Zeng, Y. Tian, X. Dong, L. Huang, H. Zeng, Z. Lin, G. Zou, *Chem. Mater.* **2024**, *36*, 2138.
[29] M. Li, X. Zhang, Z. Xiong, Y. Li, Y. Zhou, X. Chen, Y. Song, M. Hong, J. Luo, S. Zhao, *Angew. Chem., Int. Ed.* **2022**, *61*, e202211151.
[30] C. Jin, F. Li, Z. Yang, S. Pan, M. Mutailipu, *J. Mater. Chem. C.* **2022**, *10*, 6590.
[31] P. Li, C. Hu, J. Mao, F. Kong, *Laser Photonics Rev.* **2024**, *19*, 2401488.
[32] L. Qi, X. Jiang, K. Duanmu, C. Wu, Z. Lin, Z. Huang, M. G. Humphrey, C. Zhang, *J. Am. Chem. Soc.* **2024**, *146*, 9975.
[33] Y. Shen, M. Ding, G. Chen, Y. Luo, S. Zhao, J. Luo, *Small* **2024**, *20*, 2400549.
[34] Y. Li, Y. Zhou, B. Ahmed, Q. Xu, W. Huang, Y. Song, X. Song, B. Chen, J. Luo, S. Zhao, *Mater. Horizons.* **2024**, *11*, 4393.
[35] H. Zhou, M. Cheng, D. Chu, X. Liu, R. An, S. Pan, Z. Yang, *Angew. Chem., Int. Ed.* **2024**, *64*, e202413680.
[36] C. Jin, H. Zeng, F. Zhang, H. Qiu, Z. Yang, M. Mutailipu, S. Pan, *Chem. Mater.* **2021**, *34*, 440.
[37] M. Zhang, B. Zhang, D. Yang, Y. Wang, *Inorg. Chem. Front.* **2022**, *9*, 6067.
[38] Y. Li, K. M. Ok, *Chem. Sci.* **2024**, *15*, 10193–10199.
[39] Y. Li, K. M. Ok, *Angew. Chem., Int. Ed.* **2024**, *63*, e202409336.
[40] Q. Chen, C. Hu, M. Zhang, J. Mao, *Chem. Sci.* **2023**, *14*, 14302.
[41] M. Zhu, J. Wang, L. Hou, Y. Yuan, L. Liu, Y. Chu, C. Huang, *Inorg. Chem.* **2024**, *63*, 2289.
[42] Z. Bai, K. M. Ok, *Angew. Chem., Int. Ed.* **2024**, *63*, e202315311.
[43] C. Chen, D. Dou, Y. Bai, B. Zhang, Y. Wang, *Inorg. Chem. Front.* **2024**, *11*, 6020.
[44] C. Huang, M. Mutailipu, F. Zhang, K. J. Griffith, C. Hu, Z. Yang, J. M. Griffin, K. R. Poeppelmeier, S. Pan, *Nat. Commun.* **2021**, *12*, 2597.
[45] M. Liang, Y. Zhang, E. Izvarin, M. J. Waters, J. M. Rondinelli, P. S. Halasyamani, *Chem. Mater.* **2024**, *36*, 2113.
[46] S. Han, A. Tudi, W. Zhang, X. Hou, Z. Yang, S. Pan, *Angew. Chem. Int. Ed.* **2023**, *62*, e202302025.
[47] M. Zhang, W. Yao, S. Pei, B. Liu, X. Jiang, G. Guo, *Chem. Sci.* **2024**, *15*, 6891.
[48] X. Zhang, D. Cao, D. Yang, Y. Wang, K. Wu, M. Lee, B. Zhang, *ACS Mater. Lett.* **2022**, *4*, 572.

[49] Y. Yang, Y. Xiao, B. Li, Y. G. Chen, P. Guo, B. Zhang, X. Zhang, *J. Am. Chem. Soc.* **2023**, *145*, 22577.
[50] K. Chen, C. Lin, J. Chen, G. Yang, H. Tian, M. Luo, T. Yan, Z. Hu, J. Wang, Y. Wu, N. Ye, G. Peng, *Angew. Chem. Int. Ed.* **2023**, *62*, e202217039.
[51] J. Lu, X. Liu, M. Zhao, X. B. Deng, K. X. Shi, Q. R. Wu, L. Chen, L. Wu, *J. Am. Chem. Soc.* **2021**, *143*, 3647.
[52] J. Yin, J. Guo, H. Huo, X. Liu, X. Cheng, Z. Lin, L. Wu, L. Chen, *Angew. Chem., Int. Ed.* **2024**, *137*, e202417579.
[53] X. Cheng, S. Gao, S. W. Ng, *Acta Crystallogr. Sect. E, Struct. Rep. Online.* **2010**, *66*, o127.
[54] H. Eshtiagh-Hosseini, Z. Yousefi, M. Mirzaei, *Acta Crystallogr. Sect. E, Struct. Rep. Online.* **2009**, *65*, o2816.
[55] S. Akyuz, *J. Supramol. Chem.* **2002**, *2*, 401.
[56] M. Subha, K. Anitha, R. Jauhar, *J. Mol. Struct.* **2019**, *1179*, 469.
[57] L. J. Sham, M. Schlüter, *Phys. Rev. Lett.* **1983**, *51*, 1888.
[58] A. J. Cohen, P. Mori-Sánchez, W. Yang, *Phys. Rev. B: Condens. Matter Mater. Phys.* **2008**, *77*, 115123.
[59] J. Li, X. Liu, Q. Cao, X. Su, L. Wu, L. Chen, *J. Alloys Compd.* **2022**, *908*, 164632.
[60] L. Zhang, S. Wang, F. Zhang, Z. Yang, X. Hou, *Dalton Trans.* **2023**, *52*, 13492.
[61] Q. Wang, J. Ren, D. Wang, L. Cao, X. Dong, L. Huang, D. Gao, G. Zou, *Inorg. Chem. Front.* **2023**, *10*, 2107.
[62] H. Zhang, D. Jiao, X. Li, C. He, X. Dong, K. Huang, J. Li, X. An, Q. Wei, G. Wang, *Small.* **2024**, *20*, 2401464.
[63] D. Hidalgo-Rojas, J. García-Garfido, J. Enríquez, R. Rojas-Aedo, R. A. Wheatley, R. A. Fritz, D. P. Singh, F. Herrera, B. Seifert, *Adv. Opt. Mater.* **2023**, *11*, 2300142.
[64] M. Xue, L. Zhang, X. Wang, Q. Dong, Z. Zhu, X. Wang, Q. Gu, F. Kang, X. Li, Q. Zhang, *Angew. Chem., Int. Ed.* **2024**, *63*, e202315338.
[65] Q. Xu, Y. Liu, Q. Wu, L. Hou, Y. Li, L. Li, Z. Lin, S. Zhao, J. Luo, *Sci. China Mater.* **2023**, *66*, 3271.
[66] N. Ma, J. Chen, B. Li, C. Hu, J. Mao, *Small.* **2023**, *19*, e2304388.
[67] S. Zhao, F. Jia, K. Zhan, R. Wang, P. Tan, L. Shen, L. Wu, L. Chen, *Chin. Chem. Lett.* **2024**, 110625.
[68] J. Guo, S. Cheng, S. Han, Z. Yang, S. Pan, *Adv. Opt. Mater.* **2020**, *9*, 2001734.
[69] A. Tudi, Z. Li, C. Xie, T. Baiheti, E. Tikhonov, F. Zhang, S. Pan, Z. Yang, *Adv. Funct. Mater.* **2024**, *34*, 202409716.
[70] P. Li, C. Hu, Y. Li, J. Mao, F. Kong, *J. Am. Chem. Soc.* **2024**, *146*, 7868.
[71] Deposition numbers 2405939 (for 4HPN), 2405940 (for 4HPO), 2405941 (for 2APMN), and 2405942 (for 2APMO) contain the supplementary crystallographic data for this paper. These data are provided free of charge by the joint Cambridge Crystallographic Data Centre and Fachinformationszentrum Karlsruhe Access Structures service.
[72] SAINT, version 7.60A; Bruker analytical X-ray instruments, Inc.: Madison, WI, **2008**.
[73] O. V. Dolomanov, L. J. Bourhis, R. J. Gildea, J. A. K. Howard, H. Puschmann, *J. Appl. Crystallogr.* **2009**, *42*, 339.
[74] A. Spek, *J. Appl. Crystallogr.* **2003**, *36*, 7.
[75] J. Tauc, *Mater. Res. Bull.* **1970**, *5*, 721.
[76] S. K. Kurtz, T. T. Perry, *J. Appl. Phys.* **1968**, *39*, 3798.
[77] S. J. Clark, M. D. Segall, C. J. Pickard, P. J. Hasnip, M. I. J. Probert, K. Refson, M. C. Payne, *Z. Kristallogr.-Cryst. Mater.* **2005**, *220*, 567.
[78] J. P. Perdew, K. Burke, M. Ernzerhof, *Phys. Rev. Lett.* **1996**, *77*, 3865.
[79] M. J. Frisch, G. W. Trucks, H. B. Schlegel, G. E. Scuseria, M. A. Robb, J. R. Cheeseman, G. Scalmani, V. Barone, G. A. Petersson, H. Nakatsuji, X. Li, M. Caricato, A. Marenich, J. Bloino, B. G. Janesko, R. Gomperts, B. Mennucci, H. P. Hratchian, J. V. Ortiz, A. F. Izmaylov, J. L. Sonnenberg, D. Williams-Young, F. Ding, F. Lipparini, F. Egidi, J. Goings, B. Peng, A. Petrone, T. Henderson, D. Ranasinghe, et al., *Gaussian 09*, Gaussian, Inc., Wallingford CT, **2016**.
[80] T. Lu, F. Chen, *J. Comput. Chem.* **2012**, *33*, 580.
[81] T. Lu, *J. Chem. Phys.* **2024**, *161*, 082503.
[82] T. D. Kühne, M. Iannuzzi, M. Del Ben, V. V. Rybkin, P. Seewald, F. Stein, T. Laino, R. Z. Khaliullin, O. Schütt, F. Schiffmann, D. Golze, J. Wilhelm, S. Chulkov, M. H. Bani-Hashemian, V. Weber, U. Borštnik, M. Taillefumier, A. S. Jakobovits, A. Lazzaro, H. Pabst, T. Müller, R. Schade, M. Guidon, S. Andermatt, N. Holmberg, G. K. Schenter, A. Hehn, A. Bussy, F. Belleflamme, G. Tabacchi, et al., *J. Chem. Phys.* **2020**, *152*, 194103.

Manuscript received: March 3, 2025
Revised manuscript received: April 1, 2025
Version of record online: April 17, 2025